Clim Dyn
DOI 10.1007/s00382-011-1137-7

Observational evidence of the delayed response of stratospheric polar vortex variability to ENSO SST anomalies

R.-C. Ren · Ming Cai · Chunyi Xiang · Guoxiong Wu

Received: 21 October 2010 / Accepted: 24 June 2011

Abstract The temporal and spatial relationship between ENSO and the extratropical stratospheric variability in the Northern Hemisphere is examined. In general, there exists a negative correlation between ENSO and the strength of the polar vortex, but the maximum correlation is found in the next winter season after the mature phase of ENSO event, rather than in the concurrent winter. Specifically, the stratospheric polar vortex tends to be anomalously warmer and weaker in both the concurrent and the next winter season following a warm ENSO event, and vice versa. However, the polar anomalies in the next winter are much stronger and with a deeper vertical structure than that in the concurrent winter. Our analysis also shows that, the delayed stratospheric response to ENSO is characterized with poleward and downward propagation of temperature anomalies, suggesting an ENSO-induced interannual variability of the global mass circulation in the stratosphere. Particularly, in response to the growing of a warm ENSO event, there exist warm temperature and positive isentropic mass anomalies in the midlatitude stratosphere since the preceding summer. The presence of an anomalous wavenumber-1 in the concurrent winter, associated with an anomalous Aleutian high, results in a poleward extension of warm anomalies into the polar region, and thus a weaker stratospheric polar vortex. However, the midlatitude warm temperature and positive isentropic mass anomalies persist throughout the concurrent winter till the end of the next summer. In comparison with the concurrent winter, the strengthening of poleward heat transport by an anomalous wavenumber-2 in the next winter results in a much warmer and weaker polar vortex accompanied with a colder midlatitude stratosphere.

Keywords Polar vortex variability · ENSO · Delayed response

R.-C. Ren (✉) · C. Xiang · G. Wu
LASG, Institute of Atmospheric Physics, CAS, 100029 Beijing, China
e-mail: rrc@lasg.iap.ac.cn

M. Cai
Department of Earth, Ocean, and Atmospheric Science, Florida State University, 32306 Tallahassee, FL, USA

Present Address:
C. Xiang
National Meteorological Center, China Meteorological Administration, 100081 Beijing, China

1 Introduction

As one of the major sources for the inter-annual variability of the climate system, the El Niño-Southern Oscillation (ENSO) has been known to have considerable influence on the inter-annual variability of the stratospheric circulation particularly in the Northern Hemisphere (NH). Specifically, it was indicated that the NH stratospheric vortex tends to be anomalously weak/strong during warm/cold ENSO winters in data (van Loon et al. 1982; Labitzke and Hvan 1989; Camp and Tung 2007) and in model simulations (Hamilton 1995; Sassi et al. 2004; Manzini et al. 2006; García-Herrera et al. 2006). Model simulations by Taguchi and Hartmann (2006) also showed that Stratospheric Sudden Warming (SSW) events during warm ENSO are twice as frequent as during cold ENSO, due to the increased wave activity in the stratosphere. However, some evidence indicates that the relationship between ENSO and the polar stratospheric variability may not be robust or statistically significant (Wallace and Chang 1982; van Loon and Labitzke 1987; Hamilton 1993). The difficulties in establishing the

Published online: 09 July 2011

relationship between ENSO and the extra-tropical stratospheric circulation have been attributed to the entangled signals of ENSO and Quasi Biannual Oscillation (QBO) in the extra-tropical stratosphere (Wei et al. 2007; Garfinkel and Hartmann 2007, 2008, Calvo et al. 2009) and the limited data length (Wallace and Chang 1982). Nevertheless, the composite results by Garfinkel and Hartmann (2007, 2008) still confirmed that ENSO does have a significant effect on the stratospheric polar vortex. By applying a Linear Discriminant Analysis method, Camp and Tung (2007) established a significant relationship between the 10-50 hPa winter-mean temperature and the ENSO phase. They also indicated that the ENSO effect is unlikely to be smaller than the QBO effect, but it takes a spatial form that is almost orthogonal to that of QBO. By analyzing the model results with sufficient data length and without QBO variability, Manzini et al. (2006) and García-Herrera et al. (2006) identified a significant relationship between ENSO and the polar vortex variability. They showed that warm ENSO tends to induce a PNA-like pattern and enhance wavenumber-1 in the stratosphere, thus resulting in the polar warming during the late winter to early spring. By concerning mainly on the mature phase of ENSO, these results basically suggest a concurrent impact of ENSO on the stratospheric circulation.

However, there are also some evidences, showing that the stratospheric response to ENSO identified in the concurrent winter of the mature phase of ENSO, may not reflect the strongest effect of ENSO in the extra-tropical stratosphere. For example, Manzini et al. (2006) noticed a time lag of the polar warming in the lower stratosphere with respect to the upper stratosphere, following a warm ENSO phase. García-Herrera et al. (2006) indicated that the maximum warming response in the stratosphere to warm ENSO forcing, does not appear in the month of the maximum Niño3.4 value, but lags for several months. And Chen et al. (2003) identified a maximum significant correlation between ENSO and the meridional EP flux divergence at 30 hPa when ENSO leads the EP flux by about three seasons. These results seem to suggest a lagged relationship between ENSO and the maximum extratropical stratospheric response or a possible delayed impact of ENSO on the stratosphere. The delayed effect of ENSO on the tropical atmosphere was identified in numerous early studies. It was found that the maximum correlation between the zonal-mean tropical temperature and the ENSO SST occurs when the eastern Pacific ENSO SST forcing leads by one to two seasons (Newell and Weare 1976; Angell 1981; Reid et al. 1989; Yulaeva and Wallace 1994). Also the zonal-mean tropical 200 hPa height response in the following summer after the peak phase of ENSO is found appreciably stronger than that in the preceding summer, despite of the weaker ENSO SST forcing in the following summer (Kumar and Hoerling 2003). The delayed tropical atmospheric response was attributed to the tropical oceans lagged response to ENSO (Kumar and Hoerling 2003). Following the ENSO-related SST signal peaked in the northern winter in the eastern Pacific, the SST anomalies in the Indian-Western Pacific (Hsiung and Newell 1983; Pan and Oort 1983; Lanzante 1996; Lau et al. 2005 and references there in) as well as that in the tropical Atlantic (Enfield and Mayer 1997; Huang et al. 2002; Ding and Li 2011 and references there in) attain their maximum amplitude 1–2 seasons later. They are remotely forced by ENSO through a series of atmospheric and ocean processes involving the "atmospheric bridge" spanning the Pacific and Indian Ocean (Lau and Nath 2003; Klein et al. 1999), the anomalous Walker circulation (Saravanan and Chang 2000) and the PNA-like teleconnection pattern (Handoh et al. 2006) spanning the Pacific and the tropical Atlantic. The delayed change of SST in the Indian and the Atlantic sectors also results in an increase in zonal homogeneity of the tropical SST anomalies and the related tropical atmospheric response (Kumar and Hoerling 2003). In relation to the zonally homogeneous tropical response that increases after the peak phase of ENSO, prominent response with the opposite polarity to the tropical response was identified in the midlatitudes band around 40°N in the following spring to summer (Kumar and Hoerling 2003; Lau et al. 2005). Lau et al. (2005) indicated that this midlatitude response was mainly forced by SST forcing in the tropical eastern Pacific and could be modulated by the delayed SST forcing in the Indian-Western Pacific. Nevertheless, this opposite signed response signal is clearly seen in the midlatitudes throughout the following spring and summer after the mature phase of a warm ENSO (Fig. 5 in Kumar and Hoerling 2003). In these ways, the information of the ENSO forcing is passed to the extratropical atmosphere 1–2 seasons later.

The existence of the seasons delayed effect of ENSO on the troposphere may give rise to a possible lagged response in the extratropical stratosphere. But currently,there are few studies about how tropical ENSO forcing could induce a lagged extratropical stratospheric response. The difficulties in understanding the lagged relationship between ENSO and the stratospheric variability are also due to the phase locking of the stratospheric variability to the annual cycle, namely that the polar vortex and the associated variations generally diminish in summer. In addition, most of the existing evidence emphasizes a concurrent response in winter of the mature phase of ENSO, and less attention has been given to the stratospheric response with respect to different phases of ENSO event. The main objective of this study is to attempt to address the following questions concerning the temporal and spatial relationship between ENSO and the stratospheric variability: Does a significant

lagged response in the extratropical stratosphere to ENSO exist? If yes, what's the mechanism that links ENSO forcing to the stratospheric variability? How to understand the relative importance between the concurrent response and the possible lagged response in the stratosphere? The answers to these questions would help to advance our understanding of the relationship between ENSO and the interannual variability of the stratosphere.

2 Data

The monthly Niño3 anomaly index from January 1950 to December 2009, obtained from http://www.cpc.noaa.gov/data/indices/ is used to define the temporal variation of the tropical ENSO. The 2° × 2° gridded monthly SST fields are from the NOAA-Extended-Reconstructed SST V3b dataset covering the period from January 1949 to December 2009 (Reynolds et al. 2002). The monthly SST anomalies are obtained by removing the climatological annual cycle at each grid point.

To define the stratospheric polar vortex oscillation variability, we choose the Northern Annular Mode (NAM) index developed by Baldwin and Dunkerton (2001); http://www.nwra.com/resumes/baldwin/nam.php). The monthly NAM index was obtained by performing monthly averaging on the original daily values. As already indicated by previous studies and will be shown in this study, the NAM and ENSO are generally negatively correlated. For easy reference of the lead/lag correlation, we reverse the sign of the NAM index and use NAM$^-$ to denote negative NAM in this study. As a result, NAM$^-$ and ENSO are generally positively correlated.

The monthly circulation anomalies such as temperature, wind and geopotential height are obtained from the ERA40 reanalysis data fields at 18 standard pressure levels from 1,000 to 10 hPa covering the period from September 1957 to August 2002 (Uppala et al. 2005). The mass anomaly fields between adjacent isentropic surfaces are derived from the isentropic data fields at 12 isentropic surfaces (θ = 300, 315, 330, 350, 370, 395, 430, 475, 530, 600, 700, 850 K) of the same data set.

To filter out the dominant QBO signal in the tropics, as well as the possible QBO-related effects in the extra-tropics, we first derive the QBO index at each level above 100 hPa from the zonal-mean anomalies subject to a 7-month running mean at the equator. We next regress the circulation anomalies at each grid point against the QBO index at the same level. Then we remove the resulting regressed anomalies from the original monthly anomalies level by level. This procedure is applied separately in the mass, temperature, zonal wind and geopotential anomaly fields to remove the QBO signal from these data. For the NAM$^-$, we simply filter out the signal in timescale between 24 and 32 months to remove the possible QBO effect.

3 Temporal lagged relationship between ENSO and the polar vortex variability

3.1 Temporal lagged correlation between the Niño3 and the NAM$^-$ indices

It is known that the polar vortex oscillation is primarily a seasonal timescale phenomenon but with considerable interannual variability, and ENSO evolves mainly on timescale of several years. Though the interannual variability of the polar vortex oscillation is relatively much weaker than its seasonal variability as shown in previous studies and will be shown below, it is by no means negligible and is important for understanding the ENSO's effect on the climate variability. To explore the possible linkage of the interannual variability of the polar stratosphere to tropical ENSO anomalies, we perform cross-spectrum analysis (http://www.lasg.ac.cn/staff/ljp/Eindex.html) on the Niño3 and NAM$^-$ indices at each pressure level. Shown in Fig. 1 are the coherency spectrum and the lag-length spectrum from 1,000 to 10 hPa. The coherency spectrum is analogous to the square of correlation coefficient except that it is a function of frequency, and the lag-length spectrum measures the phase relationship between the two indices over the frequency span. It is clearly seen that, over the period span from 19 to 96 months, the significant coherency only appears in the timescale of around 4 years. The significant correlation between Niño3 and the NAM$^-$ indices is seen throughout the upper troposphere to the stratosphere, and peaks in the lower stratosphere around 150 hPa (Fig. 1a). From the lag-length spectrum shown in Fig. 1b, we know that the significant coherency basically indicates a lagged, rather than a simultaneous relationship between Niño3 and the NAM$^-$ indices. Specifically, on the inter-annual timescale of about 4 years, ENSO anomalies and the stratospheric variability are significantly correlated when Niño3 leads the NAM$^-$ by about 9–11 months or approximately by a quarter of the period length. Regarding that ENSO generally peaks in winter and the stratospheric NAM$^-$ is dominated by winter variability, the existing time lag of a quarter period may just be the manifestation of the possible relationship between the ENSO anomalies in the concurrent winter and the stratospheric variability in winter season of the next year. Consistently, the corresponding quadrature spectrums (not shown) also exhibit the strongest spectrum peak over this period.

To demonstrate the temporal lagged relationship more effectively and to focus only on the winter season variability of both ENSO and the NAM$^-$, Fig. 2 shows the

lead/lag regression of the NAM$^-$ from 1000 to 10 hPa against the 3–5 years band-pass filtered Niño3 index in winter months (NDJFMA). Consistent with the time lag for the significant coherency shown in Fig. 1, the maximum positive anomalies of the NAM$^-$ indices from the upper troposphere to the stratosphere do appear when Niño3 leads by about 1 year (9–11 months), though relatively weaker positive anomalies also exist in the concurrent winter months when Niño3 leads by about 2 months. In other words, on average, the polar vortex is anomalously weaker both in the concurrent winter-spring season and the next winter season following a warm ENSO and vice versa. However, the strongest polar stratospheric anomalies are in the next winter season after the mature phase of ENSO, especially in the stratosphere above 100 hPa. Apparently, the relatively weaker response of the NAM$^-$ in the concurrent winter-spring (month +2) seen in Fig. 2, just confirms what most of the previous studies have identified by focusing on the mature phase of ENSO, that warm ENSO induces an anomalously warmer and weaker polar vortex and vice versa (Hamilton 1995; Sassi et al. 2004; Manzini et al. 2006; García-Herrera et al. 2006; Camp and Tung 2007).

Since about 87% of the total variance of the monthly Niño3 index is associated with the 3–5 year timescale, the results obtained in this study by using the 3–5 year filtered Niño3 can essentially represent the lagged stratospheric effects of ENSO. For easy reference, below we simply refer the 3–5 year filtered Niño3 index in winter months as the winter Niño3 index, and the 3–5 year filtered NAM$^-$ indices as the interannual NAM$^-$ indices.

3.2 Mutual reproduction of the spatial patterns between ENSO and the polar vortex oscillation

By regressing the tropical SST anomalies against the winter (NDJFMA) Niño3 index, the canonical El Niño SST pattern can be obtained (Fig. 3a). Comparing this pattern with the tropical SST anomaly pattern obtained from their lead correlations with the interannual NAM$^-$ index in winter (ONDJFM) stratosphere (averaged in 10–100 hPa) at a 11 months lag (Fig. 3b), it is found that they closely resemble each other, suggesting that the leading SST anomaly pattern with respect to the NAM$^-$ is related to a mature ENSO phase. It is also noted that the amplitude in Fig. 3b is only about half of that in Fig. 3a, which may

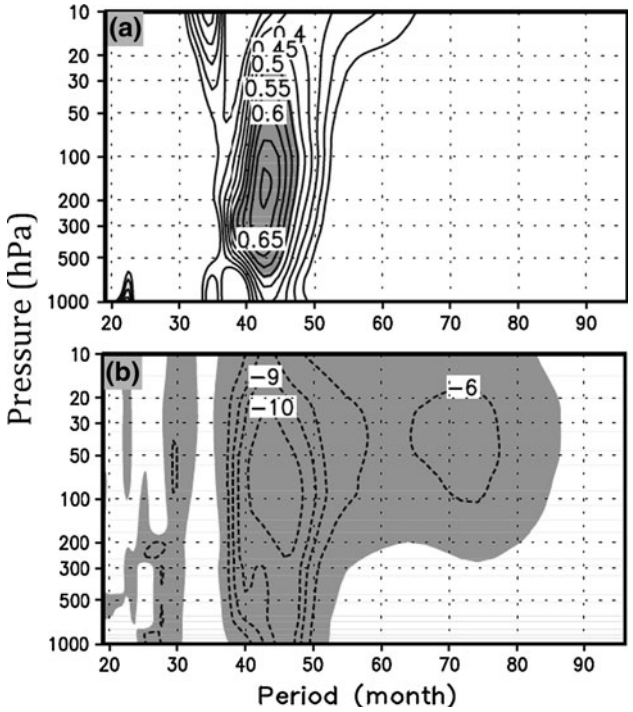

Fig. 1 Coherency spectrum (**a**) and lag-length (month) spectrum (**b**) between the Monthly Niño3 index and the NAM$^-$ indices from 1,000 to 10 hPa. Shaded in (**a**) marks the 95% confidence level of the coherency, and in (**b**) marks the negative values of the lag-length. Contour values smaller than 0.2 in (**a**) and -6 in (**b**) are skipped for clarity. Positive/negative values of the lag-length in (**b**) denotes the time in month by which the Niño3 lags/leads the NAM$^-$

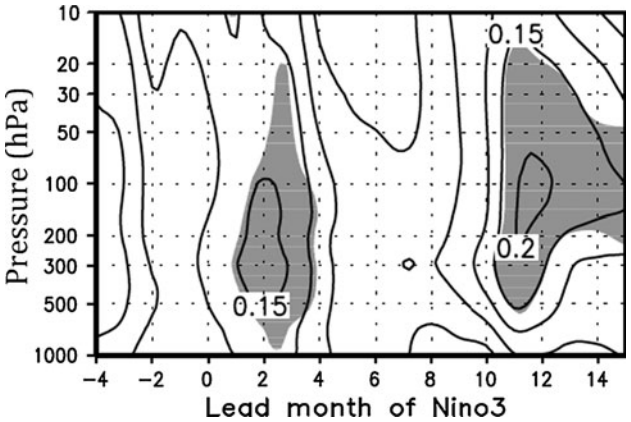

Fig. 2 Lead/lag regression of the NAM$^-$ indices from 1,000 to 10 hPa, against the 3–5 year filtered Niño3 in winter (NDJFMA) months. *Shaded areas* denote the 95% confidence level. For any two time series $X(t)$ and $Y(t)$. Following Trenberth (1984) and Katz (1982), we first construct AR(1) auto-regressive time series $X'(t)$ from the original time series $X(t)$ using $X'(1) = X(1) - \bar{X}$ and $X'(t) = X(t) - \bar{X} + C_{xx}(1)(X(t-1) - \bar{X})$ for t = 2, 3 … N, where $\bar{X}$ is the time mean of $X(t)$ and $C_{xx}(1)$ the lag-1 auto correlation of $X(t)$. Similarly, we apply the AR(1) to construct $Y'(t)$ from $Y(t)$. We then apply the method of Davis (1976) to estimate the effective degree of freedom (EDOF) in the correlation between $X(t)$ and $Y(t)$ according to $EDOF = N\left[\left(1 - \frac{|\tau|}{N}\right)\sum_{\tau=-N+1}^{N-1} C_{xx}(\tau)C_{yy}(\tau)\right]$, where the lag-$\tau$ auto correlations $C_{xx}(\tau)$ and $C_{yy}(\tau)$ are calculated from $X(t)$ and $Y(t)$ for $\tau \leq 1$ but from $X(t)$ and $Y(t)$ for $\tau > 1$. We use the same procedure to estimate EDOFs in testing the significance of the cross-correlations between the indices and the circulation anomalies in the remaining part of the paper

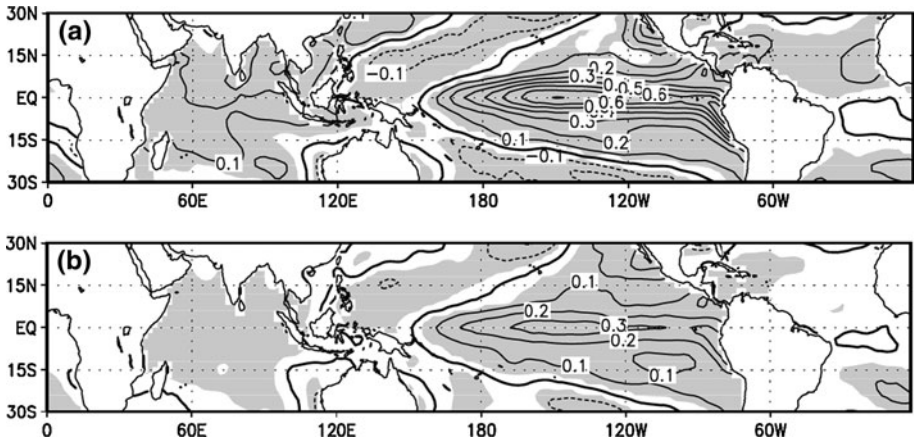

Fig. 3 Concurrent regression pattern of the tropical SST anomalies (unit: K) against the filtered Niño3 index in winter month (**a**) and the leading regression pattern against the 3–5 year filtered stratospheric NAM$^-$ index (10–100 hPa) in winter (ONDJFM) months at a 9–11 months lag (**b**). Shaded are the areas above the 95% confidence level

further suggest that part of the tropical ENSO SST variability is connected to the interannual variability of the winter stratospheric NAM$^-$ at about a 11-months lag. In other words, about 11 months prior to the positive phase of the NAM$^-$ on the interannual timescale, the tropical SST tends to exhibit a mature warm ENSO pattern. Conversely, about 11 months prior to the negative phase of the NAM$^-$, the tropical SST tends to exhibit a mature cold ENSO pattern.

Shown in Fig. 4a, b are the typical zonal mean spatial patterns related to stratospheric polar vortex oscillation event obtained by regressing the monthly zonal mean anomalies against the winter month (ONDJFM) NAM$^-$ in the stratosphere (100–10 hPa). The patterns highly resemble the regression patterns (except the reversed sign) against the daily NAM index (Thompson and Wallace 2000) and that against the daily Polar Vortex Oscillation (PVO) Index (Ren and Cai 2007). Specifically, positive peak of NAM$^-$ events is characterized with large amplitude of polar stratospheric warming (Fig. 4a) and easterly anomalies of the polar jet (Fig. 4b). The strongest warming center is located around the layer of 50–70 hPa, which coincides with the altitude of the climatological mean action center of the polar vortex. Both the temperature and the zonal-mean zonal wind anomalies exhibit an out-of-phase relationship between the lower and the higher latitudes, especially in the stratosphere. Similarly, the zonal-mean spatial patterns related to the interannual variation of the stratospheric oscillation, particularly on the 3–5 year timescale, are obtained by regressing the anomalies against the corresponding interannual NAM$^-$ (Fig. 4c, d). The high resemblance between Fig. 4a, c, and between Fig. 4b, d, is indicative of that the interannual variability of the stratospheric circulation is also related to winter NAM$^-$ (or PVO) events. Note that the amplitude in Fig. 4c, d is only about 1/4 of that in Fig. 4a, b, due to the dominance of the seasonal variability of the stratospheric oscillation.

To confirm the temporal lagged relationship between ENSO and the interannual variability of the stratospheric oscillation, Fig. 5 shows the zonal-mean regression patterns of the temperature and zonal wind anomalies against

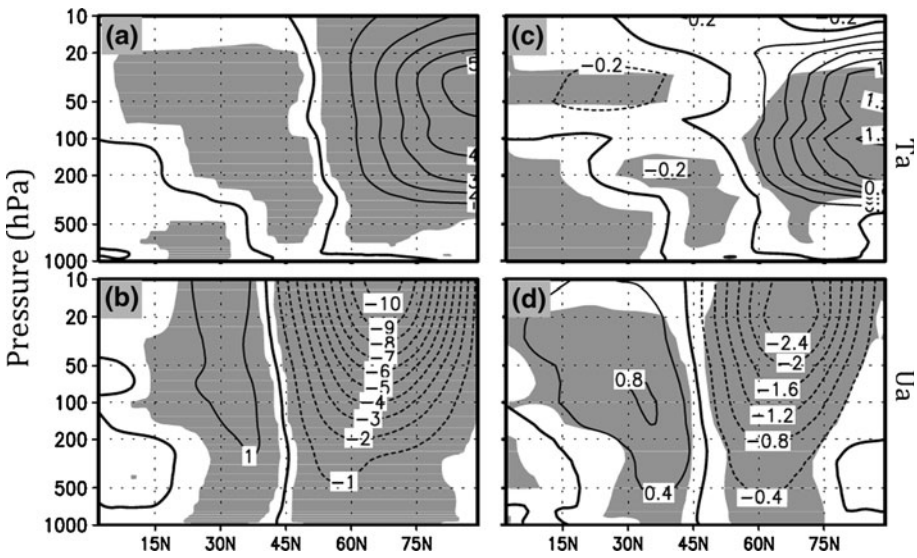

Fig. 4 Regression patterns of the zonal mean temperature (*upper*, unit: K) and zonal wind (*bottom*, unit: m s^{-1}) anomalies against the monthly NAM$^-$ (**a**, **b**) and the 3–5 year filtered NAM$^-$ (**c**, **d**) in winter (ONDJFM) months averaged in the stratosphere above 100 hPa. Shaded are the areas above the 95% confidence level

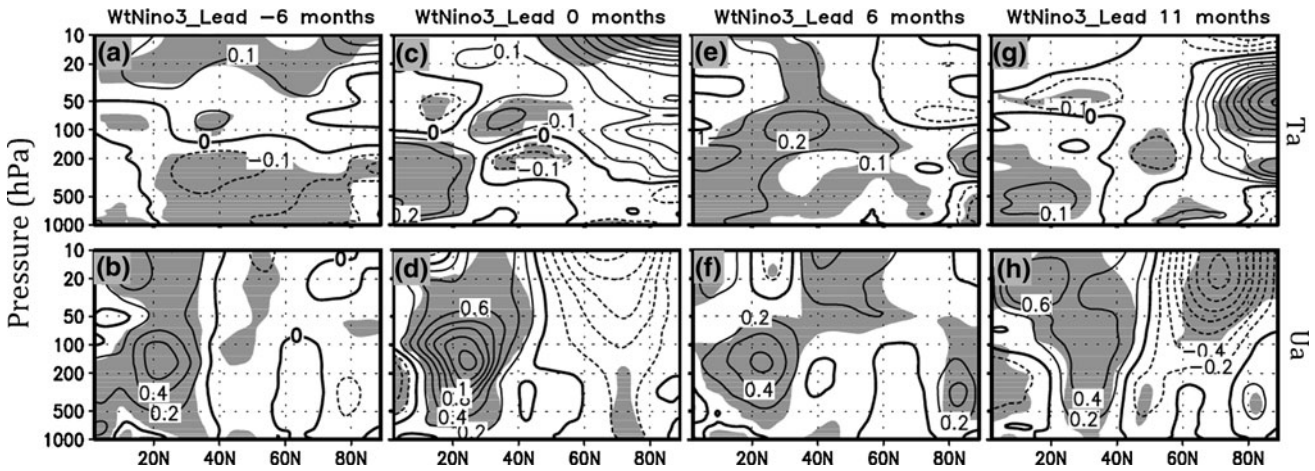

Fig. 5 Regression patterns of the zonal mean temperature (*upper*, unit: K) and zonal wind (*bottom*, unit: m s^{-1}) anomalies against the winter filtered Niño3 index leading, respectively, by −6 (**a**, **b**), 0 (**c**, **d**), 6 (**e**, **f**) and 11(**g**, **h**) months. Contour interval is 0.1 in (**a**, **c**, **e**, **g**) and 0.2 in (**b**, **d**, **f**, **h**). *Shaded* are the areas above the 90% confidence level

the winter Niño3 leading by −6 (preceding summer), 0 (concurrent winter), 6 (following summer) and 11 (next winter) months. Since the typical lag-length for the significant correlation between Niño3 and the NAM^{-} indices is about 11 months, we use the winter month (NDJFMA) Niño3 index in obtaining the lagged regression patterns to effectively capture the winter variability of the stratospheric oscillation in ONDJFM. Comparing Fig. 5c, d, g, h, it is seen that in both the concurrent (zero-lag time, Fig. 5c, d) and the next winter season (11-months lag, Fig. 5g, h) relative to the mature phase of ENSO, there exist warming and easterly anomalies in the extratropical stratosphere. But they are obviously weaker and less statistically significant in the concurrent winter than that in the next winter season. The polar warming anomalies in Fig. 5c are seen only in upper layers above 20 hPa, and the pronounced and significant response in the concurrent winter is found mainly in the tropics and the subtropics, namely the tropical tropospheric warming (Fig. 5c) and the strong westerly anomalies over the subtropical jet (Fig. 5d), which are obviously the direct consequence of the enhanced tropical convection and the tropospheric Hadley circulation associated with the warm ENSO SST anomalies. In contrast, the stronger and more significant anomalies in Fig. 5g, h are mainly in the extratropics. Moreover, the main features of the lagged regression patterns in Fig. 5g, h closely resemble that in Fig. 4, suggesting that the lagged responses in the extratropical stratosphere to ENSO are indeed related with winter NAM^{-} (or PVO) events. Particularly, the strongest polar warming north of 60°N in the stratosphere is centered at about 50 hPa, and the temperature and zonal wind anomalies both exhibit an out-of-phase relationship between the lower and the higher latitudes as in Fig. 4. The finding here also independently supports the findings by Taguchi and Hartmann (2006) that the warm ENSO-induced stratospheric response is related to Sudden Stratospheric Warming events. Comparing Fig. 5g, h with Fig. 4c, d, it can be roughly estimated that most part (above 2/3) of the 3–5 year timescale variability in the winter extratropical stratosphere is related to the ENSO-induced lagged variations.

In the preceding (Fig. 5a, b) and the following summer (Fig. 5e, f) relative to the mature phase of ENSO, the atmospheric response in the extratropical stratosphere is remarkably weaker due to the lack of stratospheric oscillations in summer months. Nevertheless, the atmospheric response in the following summer (Fig. 5e, f) is relatively stronger than that in the preceding summer (Fig. 5a, b) especially in the tropics and the midlatitudes, despite of the relatively weaker ENSO SST anomalies in the following summer. This manifests the delayed effect of ENSO on the tropical and the midlatitude atmosphere in the troposphere (Kumar and Hoerling 2003; Lau et al. 2005). It is noteworthy that there are significant warming anomalies (25–40°N above 200 hPa, Fig. 5e) accompanied with westerly anomalies (35–50°N above 200 hPa, Fig. 5f) in the midlatitude stratosphere in the following summer after the mature phase of a warm ENSO. This stratospheric warming signal seems to first appear as early as in the preceding summer (Fig. 5a, b), and is gradually getting strengthened accompanying the growing of the warm ENSO until the following summer (Fig. 5c–f), resulting in a significantly warmer midlatitude stratosphere in the following summer season. It will be shown in the next two sections that, the stratospheric warming anomalies in the midlatitudes in the following summer are important for the maximum response occurred in the following winter polar stratosphere after the mature phase of the warm ENSO.

The mutual reproduction between the concurrent regression patterns against the winter NAM^{-} index and the lag regression patterns against the winter Niño3 index, and the mutual reproduction between the concurrent regression pattern of the tropical SST anomalies against the winter Niño3 and the lead regression patterns against the winter NAM^{-}, have confirmed the temporal lagged relationship identified in the previous section between ENSO and the extratropical stratospheric variability. Specifically, following a warm ENSO, the polar stratosphere is anomalously warmer accompanied with a weaker polar stratospheric westerly jet both in the concurrent and the next winter season. However, the strongest extratropical response is in the next winter season when ENSO leads by about 11 months. The reverse can be said for the cold phase of ENSO.

4 Association with the inter-annual variability of the global mass circulation

The global mass circulation spanning from the equator to the winter pole, is forced by both the meridional diabatic heating/cooling gradient and the wave activity in the extratropics (Johnson 1989 and references therein). It consists of a poleward warm air branch in the upper layer and an equatorward cold air branch in the lower layer. It has been found that the intra-seasonal variability of the global mass circulation in both the Northern and the Southern Hemisphere, is intimately related to the intra-seasonal variation of the stratospheric Polar Vortex Oscillation in winter season (Cai and Ren 2006, 2007; Ren and Cai 2008). Specifically, the strengthening or weakening of the warm branch of the global mass circulation is characterized with simultaneous poleward and downward propagation of the stratospheric circulation anomalies. The arrival of warm (or positive isentropic mass) anomaly signal in the polar region corresponds to a weakened stratospheric polar vortex, and vice versa. Isentropic mass anomalies in a latitude band (say inside the polar circle) reflect both the meridional mass circulation (a non-local factor) and the local diabatic heating/cooling anomalies; the local and non-local processes are intimately coupled because the arrival of warm or cold air mass would imply diabatic heating or cooling anomalies through longwave radiative and irreversible mixing processes.

To examine the possible association of the lagged relationship between ENSO and the stratospheric variability with the inter-annual variability of the Northern Hemispheric mass circulation, next we display the ENSO-induced temporal evolution of the mass anomalies in the stratosphere. Shown in Fig. 6b is the lead/lag regression of the zonal averaged isentropic mass anomalies in the stratospheric isentropic layer between 473 and 700 K against the winter Niño3 index with the lead-time of the index varying from −18 to +18 months. The auto-regression of the index is shown in Fig. 6a. In the initiating stage of a warm ENSO event (lead month −12 to −9) in the preceding winter season, positive mass anomalies prevail in the tropical and subtropical stratosphere whereas negative mass anomalies prevail in the polar stratosphere. A dipole pattern with opposite polarity is found in the ending

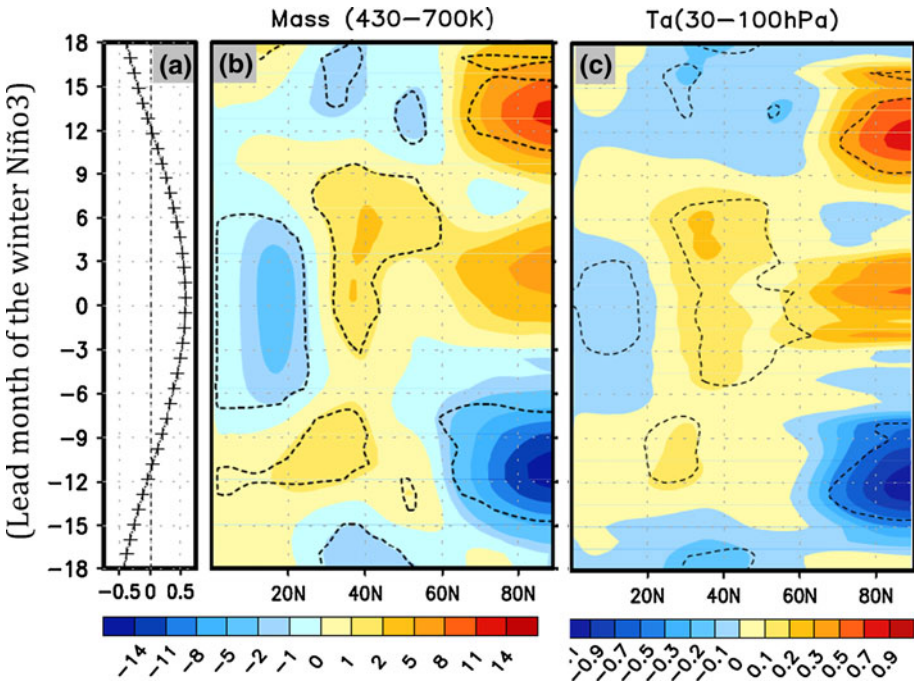

Fig. 6 Lead/lag regression of the stratospheric mass anomalies in isentropic layer between 430 and 700 K (**b**, *shaded*, unit: kg m^{-2}) and the stratospheric temperature anomalies averaged between 30 and 100 hPa (**c**, *shaded*, unit: K), against the winter filtered Niño3 index, with the lead-time the index varying from −18 to +18 months. *Dashes mark* the 90% confidence levels. The auto-regression of the Niño3 index is shown in (**a**)

stage of a warm ENSO in the next winter season (lead month +12). During the mature stage of ENSO from the preceding summer (lead month −6) to the following summer season (lead month +6), negative mass anomalies appear in the tropics and significant positive mass anomalies persist in the midlatitudes. Though there also appear stronger positive mass anomalies in the polar stratosphere in the concurrent winter, the change in meridional distribution of mass anomalies from the lead-time −12 to +12 months is still indicative of a slowly poleward propagating signal of positive mass anomalies on the timescale of ENSO. As for the intra-seasonal variability of the mass circulation (Cai and Ren 2007), this spatial and temporal evolution of the mass anomalies is indicative of a strengthening of the poleward air mass transport, or a strengthening of the warm air branch of the NH winter global mass circulation accompanying a warm ENSO. Specifically, in response to the growing of a warm ENSO event, the poleward mass transport from the tropics to the midlatitudes is seen first enhanced since the preceding summer (lead month −6), which could be attributed to the contribution of the tropical diabatic heating to the meridional circulation in the stratospheric tropics (Plumb and Eluszkiewicz 1999). The increased positive mass anomalies in the midlatitudes, plus the wave-driven meridional circulation in the extratropics during the concurrent winter season (lead month −3 to +3), are favorable for a stronger poleward mass transport in the extratropics. However, in the following spring-to-summer season (lead month +3 to +7), the extratropical poleward mass circulation seems to retreat back due to its seasonality, while the positive mass anomalies in the midlatitudes are further strengthened, suggesting a still stronger poleward mass circulation in the lower latitudes. During the next winter season, the strongest polar mass anomalies and the meridional negative-positive dipole pattern of mass anomalies suggest that the poleward mass transport is the strongest.

The lead/lag regression of the zonal-mean temperature anomalies in the stratosphere (30–100 hPa) is shown in Fig. 6c. It is seen that the stratospheric temperature anomalies are positively correlated with the mass anomalies and display a similar temporal and spatial evolution as in Fig. 6b. Consistent with the strengthening of the mass circulation accompanying a warm ENSO event, the entire stratosphere tends to be anomalously warmer, and the meridional distribution of the temperature anomalies also evolves from a warm-cold dipole pattern in the initiating stage in the previous winter (lead month −12), to an opposite cold-warm dipole pattern in the ending stage of a warm ENSO event in the next winter (lead month +12 to +15). Corresponding to the positive mass anomalies in the midlatitude stratosphere during the mature stage of the ENSO, warming anomalies also prevail in the midlatitudes from the preceding summer to the following summer season, as already seen in Fig. 5c, e. In the concurrent winter, though there is poleward extension of the warming anomalies into the polar region that results in a warmer polar stratosphere, much stronger polar warming anomalies accompanied with a colder midlatitude stratosphere are seen till the next winter. In other words, the winter polar stratosphere is anomalously warmer in both the concurrent and the next winter season, but the stronger polar warming anomalies are in the next winter season after the mature phase of ENSO, coinciding with the stronger positive mass anomalies in the polar stratosphere in the next winter.

The slowly poleward propagation of both the warm temperature and positive isentropic mass anomaly signals in the stratosphere already suggests a strengthened poleward mass circulation accompanying a warm ENSO. Next we further show that the strengthening of the mass circulation is also accompanied with simultaneous downward propagation of circulation anomalies in the extratropical stratosphere. Figure 7 displays the time-vertical cross-section of the regressed extratropical temperature anomalies against the winter Niño3. It is seen that, the seasonal timescale downward propagation of warmer temperature anomalies is evident in both the concurrent winter (0 month) and the next winter (+12 month) season, accompanying the strengthened poleward mass circulation (Fig. 6b). But the vertical span of the downward propagation in the next winter is much deeper and the strength of the anomaly signal in the mid-to-lower stratosphere is relatively stronger than that in the concurrent winter. It is seen that the main warmer anomaly signal in the concurrent winter seems to remain in the upper layer above 20 hPa, while the main warmer anomaly signal in the next winter is propagated down to the lower stratosphere and even to the troposphere. As a result, a slowly downward propagation of temperature anomaly signal can also be identified from the upper stratospheric layer during the initiating stage (month −12) to the lower stratospheric layer and the troposphere during the ending stage of a warm ENSO (month +12). In other words, the vertical distribution of the temperature anomalies evolves from a prevailing warm-cold pattern

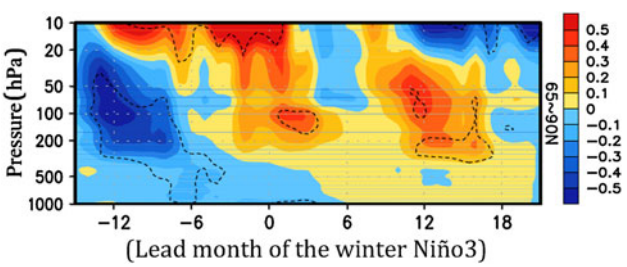

Fig. 7 Lead/lag regression of the zonal-mean temperature anomalies averaged north of 65°N (*shaded*). *Dashes mark* the 90% confidence levels

during the initiating stage of ENSO (before month +0) to an opposite cold-warm pattern in the ending stage of ENSO (after month +10). The slowly downward propagation of the warmer anomaly signal, accompanied with the slowly poleward propagation seen in Fig. 6, further supports our view of an interannual timescale strengthening of the meridional mass circulation induced by warm ENSO.

The wave-driven Brewer-Dobson circulation defined in the winter stratosphere also involves the meridional air mass transport between the tropics and the extratropics, and could be modulated by the changes of the diabatic heating/cooling in the tropics/extra-tropics (Holton et al. 1995; Mohanakumar 2008). And it is coincidently poleward and downward outside of 30°N and 30°S (Mohanakumar 2008). Thus it is logical to anticipate that, on the interannual timescale, the strengthening/weakening of the global mass circulation in the stratosphere, would coincide with the speeding-up/slowing-down of the Brewer-Dobson circulation. In García-Herrera et al. (2006), the warm-ENSO-induced stratospheric responses were related to the enhancement of the Brewer-Dobson circulation.

5 Delayed thermal response in the midlatitude stratosphere in the following spring-to-summer

As already shown in Figs. 5, 6, there exist significant warm temperature and positive mass anomalies in the midlatitude stratosphere from the preceding to the following summer accompanying a warm ENSO. This thermal anomaly signal can be related to the strengthening of the poleward mass circulation. To further show the close linkage of this midlatitude anomaly signal to the lagged maximum polar response in the next winter, the lead/lag regression patterns of the temperature anomalies in the stratospheric layer (30–100 hPa) against the winter Niño3 index leading by −6, 0, +3, +6 and +11 months are displayed in Fig. 8. Consistent with the zonal-mean patterns in Figs. 5, 6, it is seen that warming anomalies in the midlatitudes, particularly from the Eurasia to the Northern Pacific, have already established in the preceding summer (−6 month, Fig. 8a) in response to the growing of a warm ENSO. In the concurrent winter when planetary waves begin to be active in the stratosphere, warmer (or positive air mass) anomaly signal also appears in the higher latitudes over the Northern Pacific region, but the rest of the polar stratosphere is still occupied by cold temperature anomalies (Fig. 8b). This corresponds to an anomalous Aleutian high (Fig. 10) in the stratosphere and the minor weakening of the polar vortex then. In the following spring and summer (Fig. 8c, d), the warming anomaly center over the Aleutian region is gradually diminished, but the warming anomalies in the midlatitudes remain prominent and become zonally homogeneous. During the next winter season, the warming anomaly signal is shifted into the polar region, resulting in a warmer polar vortex surrounded by cold anomalies outside of the polar region. Therefore, the persistence of the zonally homogeneous warming anomalies in the midlatitudes in the following spring-to-summer seems to be a precondition for the much warmer polar vortex in the next winter.

Previous studies showed that the delayed atmospheric response in the troposphere to a warm ENSO is characterized with warming (and positive height) anomalies in the tropics accompanied with cooling (and negative height) anomalies in the midlatitudes in the following summer; and they tend to exhibit a zonally homogeneous feature in response to the zonally homogeneous tropical SST anomalies following the mature phase of ENSO (Kumar and Hoerling 2003; Lau et al. 2005). From the zonal-mean patterns in Fig. 5 we have already seen that, coupled with the zonal-mean stratospheric warming anomalies in the midlatitudes are the significant cooling anomalies just below in the upper troposphere. The cooling anomalies accompany the development of the tropical tropospheric warming and the strengthening of the subtropical jet, and are centered at about 200 hPa (Fig. 5a–d). The existence of

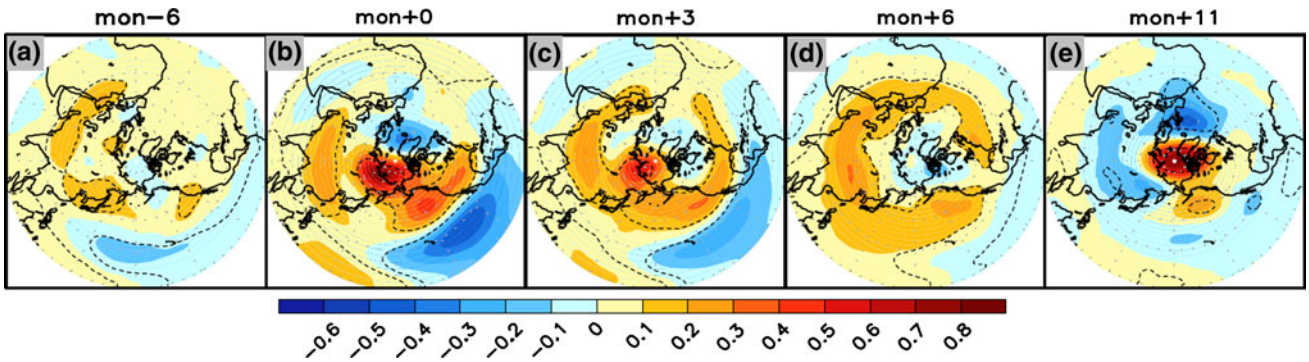

Fig. 8 Lead/lag regression patterns of the temperature anomalies in the stratospheric layer from 100 to 30 hPa (*shaded*), against the winter filtered Niño3 index leading by −6 (**a**), 0 (**b**), 3 (**c**), 6 (**d**) and 11(**e**) months. *Dashes mark* the 90% confidence level

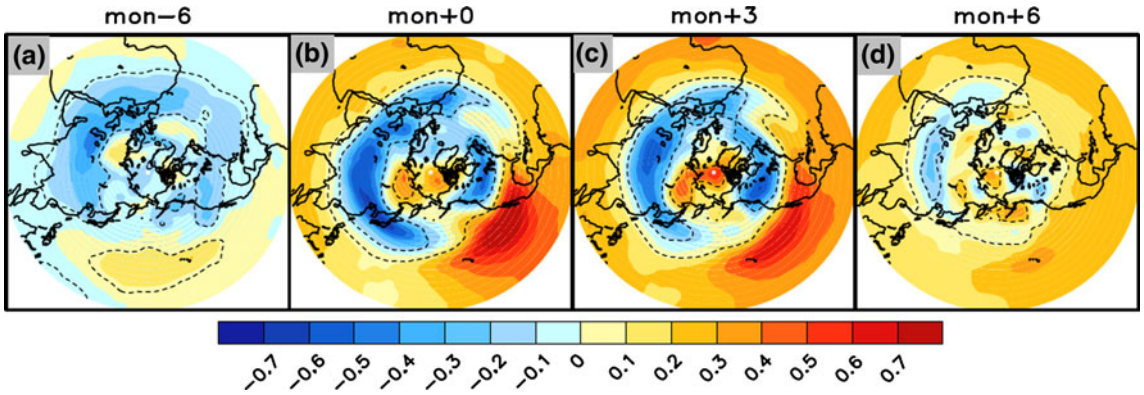

Fig. 9 Lead/lag regression patterns of the temperature anomalies at 200 hPa, against the winter filtered Niño3 index leading by −6 (**a**), 0 (**b**), 3 (**c**) and 6 months (**d**). *Dashes mark* the 90% confidence level

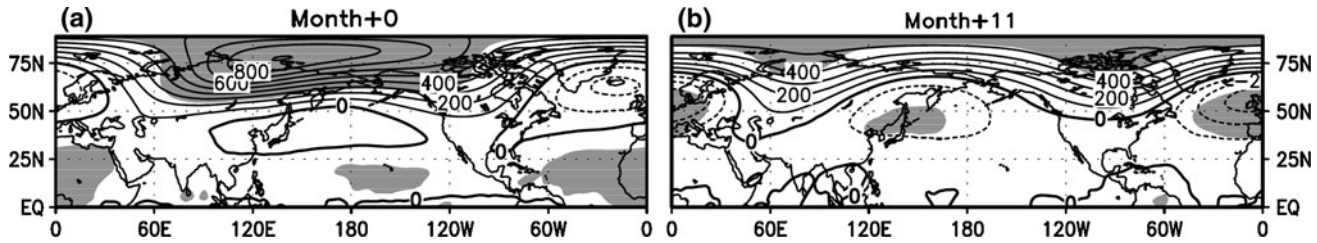

Fig. 10 Regression patterns of the geopotential height anomalies at 10 hPa against the winter filtered Niño3 index leading by 0 (**a**) and 11 months (**b**). *Shaded marks* the 90% confidence level

this cooling anomaly signal in the midlatitude is in agreement with the negative height anomalies outside of the tropics at 200 hPa identified in Lau et al. (2005) and Kumar and Hoerling (2003). As in Fig. 8, the regression patterns of the temperature anomalies at 200 hPa from the preceding summer to the following summer are displayed in Fig. 9. It is seen that, just as the warming anomalies in the midlatitude stratosphere, the cooling (or negative height) anomalies are also established in the midlatitudes as early as in the preceding summer (−6 month, Fig. 9a). Since cooling anomalies in the upper troposphere naturally represent a decrease in thickness of the atmospheric layer, the direct response to this in the stratosphere above is an increase in thickness of the stratospheric layer, as represented by the midlatitude warming anomalies seen in Fig. 8. During the concurrent winter (0 month, Fig. 9b) when ENSO matures, the cooling anomalies are strengthened accompanied with the strengthening tropical warming. In the following spring (+3 month, Fig. 9c), consistent with the increase in zonal homogeneity of the tropical warming, the midlatitude cooling anomalies also become more zonally homogeneous. Correspondingly, the increase in zonal homogeneity of the warming anomalies in the midlatitude stratosphere is also prominent, though amplitude of the stratospheric warming anomaly is slightly decreased (Figs. 8c and 9c). In the following summer (+6 month, Fig. 9d), due to the further decay of the ENSO-related tropical warming, the midlatitude cooling anomalies in the upper troposphere are significantly weakened. The much prominent weakening of the midlatitude cooling (or negative height) anomalies was also related to the tropospheric effect of the delayed Indo-Western Pacific SST warming induced by a warm ENSO (Lau et al. 2005). Despite of this, the corresponding stratospheric warming anomalies are seen even more zonally homogeneous due to the lack of meridional exchange in summer season, though local amplitude is also decreased (Fig. 8d).

6 Planetary wave activity in the stratosphere in the concurrent and the next winter

To display the association of the planetary wave activity in the stratosphere with the relatively much stronger/weaker polar response in the next/concurrent winter, the regressed height anomaly patterns at 10 hPa in the concurrent winter (month +0, Fig. 10a) and the next winter (month +11, Fig. 10b) are shown in Fig. 10. It is seen that, the extratropical stratosphere is straddled by positive height anomalies in both of the winters. However in the concurrent winter, the height anomalies are centered over the North Pacific Aleutian region, away from the North Pole. In contrast, the positive height anomalies in the next winter

(Fig. 10b) are centered closely over the North Pole with two ridges, respectively, located over the Eurasia and the America. Such change in location of the ENSO-induced height anomaly center in the extratropics naturally implies a dominant wavenumber-1 pattern in the stratosphere in the concurrent winter and a wavenumber-2 pattern in the next winter season. Garfinkel and Hartmann (2008) and Manzini et al. (2006) also indicated the increase of wavenumber-1 during the concurrent winter of mature ENSO. They also showed that the wavenumber-1 in the stratosphere was related to a Pacific-North America (PNA)-like pattern in the upper troposphere. The association of the PNA-like perturbation in the troposphere with the anomalous wavenumber-1 pattern in the extra-tropical stratosphere is documented in Itoh and Harada (2004).

The change in wave patterns in the stratosphere from the concurrent winter to the next winter can be seen more clearly in Fig. 11. In the concurrent winter (Fig. 11a, b), the wavenumber-1 component (Fig. 11a) of the height anomalies is seen about four times larger than the wavenumber-2 component in Fig. 11b. In contrast in the next winter (Fig. 11c, d), the wavenumber-1 component is substantially weakened while the wavenumber-2 component is significantly strengthened being four times larger than the wavenumber-1. It is known that an anomalous wavenumber-1 is associated with a displacement of the polar vortex off the polar area, while an anomalous wavenumber-2 is directly related to change in strength of the polar vortex or splitting of the vortex. The decreasing/increasing of the wavenumber-1/wavenumber-2 is in agreement with the maximum weakening of the polar vortex in the next winter season after the mature phase of a warm ENSO. The dominant wavenumber-1 in the concurrent winter corresponds to the relatively minor weakening of the polar vortex.

To qualitatively measure the irreversible wave effect on the anomalous meridional circulation and the related polar warming in the stratosphere, we diagnose the ENSO-induced wave-driven dynamical heating anomalies in both the concurrent and the next winters. According to Hu and Tung (2002), the dynamical heating on the mean temperature averaged over an area from latitude ϕ to the North Pole can be estimated with the zonal-mean poleward heat flux $\overline{v'\theta'}$ at latitude ϕ:

$$\frac{\partial}{\partial t}\langle\bar{\theta}\rangle \approx \left.\frac{\overline{v'\theta'}\cos\phi}{a(1-\sin\phi)}\right|_{\phi} + \langle\bar{Q}\rangle \tag{6.1}$$

where $\theta \equiv T(1000/p)^{R/Cp}$ is the potential temperature, a is the earth's radius, the terms with overbar and with prime represent the zonal-mean and the zonal deviation, respectively, and $\bar{Q}$ is the zonal-mean net radiative heating and $\langle\cdot\rangle$ denotes the area-weighted meridional average from latitude ϕ to the pole.

Here we first calculate the poleward heat flux $\overline{v'T'}$ using the monthly anomaly fields, and then we obtain the lead/lag regression of $\overline{v'T'}$ against the winter Niño3 index. Figure 12 shows the temporal evolution of the zonal-mean poleward heat flux $\overline{v'T'}$ along 60°N in the stratospheric layer above 200 hPa, for the lead-time of the Niño3 index varying from −7 to +15 months. To capture the sharp seasonality of wave activity in the stratosphere more effectively, only the winter NDJ Niño3 values are used in obtaining the lead/lag regression of the heat flux. It is seen that, accompanying the dominant wavenumber-2, the wave-driven poleward heat-flux is indeed the strongest in the next winter season, and with a much deeper vertical structure throughout the stratospheric layer above 200 hPa (around month +11). There also exists anomalous poleward heat-flux above 100 hPa in the concurrent winter (month −3 to 0) accompanying the dominant wavenumber-1, but it is much weaker and seems not statistically significant. The much stronger wave-driven poleward heat-flux and thus the stronger dynamical heating anomalies over the polar region in the next winter, manifest the dominant role of the planetary wave activity in driving the stronger poleward mass circulation in the extratropics. Therefore, it is the wave-driven poleward heat-flux

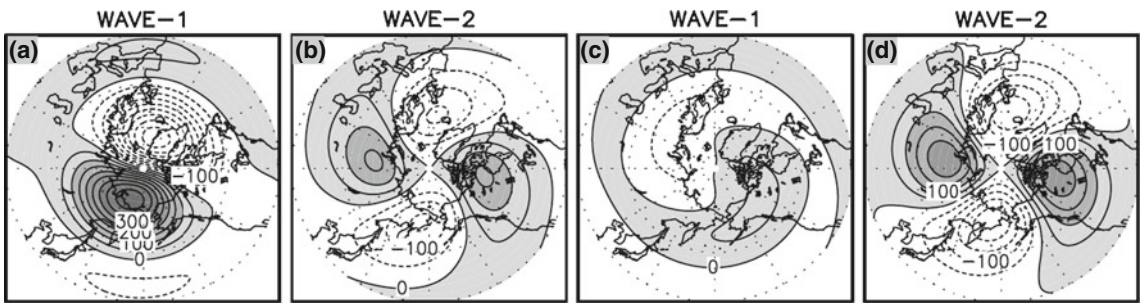

Fig. 11 The wavenumber-1 (**a**, **c**) and wavenumber-2 (**b**, **d**) components of the regressed geopotential height anomalies in Fig. 10, for the winter filtered Niño3 index leading by 0 (**a**, **b**) and 11 months (**c**, **d**). Positive areas are *shaded*

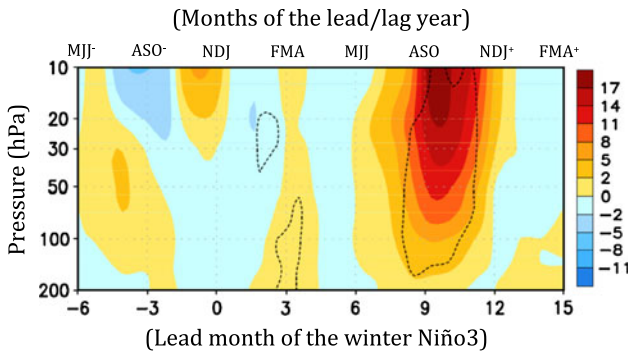

Fig. 12 Temporal evolution of the regressed zonal-mean wave-driven poleward heat flux (*shaded*, unit: K m s^{-1}) at 60°N in the stratospheric layer from 200 to 10 hPa, against the winter (NDJ) filtered Niño3 index. *Dashes mark* the 90% confidence level

associated with a stronger poleward mass circulation, and the warm (and positive isentropic mass) anomaly signal existing in the midlatitude stratosphere in the following summer, that are responsible for the strongest polar warming (weakest polar vortex) in the next winter season. Though warm (or positive mass) anomaly signal has already appeared in the midlatitude stratosphere since the preceding summer, the relatively weaker poleward heat transport by the ENSO-induced wavenumber-1 only results in the minor polar warming (or weakening of the polar vortex) in the concurrent winter.

7 Summary

This study examines the temporal and spatial relationship between ENSO SST anomalies and the extratropical stratospheric Polar Vortex Oscillation variability. In general, there exists a negative correlation between ENSO and the strength of the stratospheric polar vortex, and the significant correlation exists mainly on the timescale of about 3–5 years. And the maximum correlation is found when ENSO leads the stratospheric oscillation by about 9–11 months. Namely that, rather than in the current winter season, the maximum polar warming and the weakest polar vortex occurs in the next winter season after the mature phase of a warm ENSO and vice versa. The mutual reproduction of the spatial patterns of ENSO by the lagged winter NAM^{-} index and the polar vortex oscillation patterns by the leading winter Niño3 index confirms this temporally lagged coupling between the tropical ENSO SST and the polar stratospheric anomalies.

Our analysis also shows that the delayed stratospheric response is characterized with poleward propagation of stratospheric temperature and isentropic mass anomalies. The change in meridional anomaly patterns from the initiating stage to the ending stage of an ENSO event manifests the result of this poleward propagation. This poleward propagation is also accompanied by simultaneous downward propagation of the temperature anomalies in the extratropical stratosphere. As for the intra-seasonal variability of the polar vortex, this poleward and downward propagation of circulation anomalies suggests an interannual variability of the poleward mass circulation associated with ENSO.

Particularly, during the mature stage of a warm ENSO since the preceding summer, warm temperature and positive mass anomalies prevail in the midlatitude stratosphere. The warmer midlatitude stratosphere is favorable for a stronger wave-driven poleward heat transport in the extratropics in the following (concurrent) winter when the planetary wave forcing becomes active. However, the presence of an anomalous wavenumber-1 in the concurrent winter, associated with an anomalous Aleutian high, only results in a poleward extension of the warm anomalies into the polar region, and a minor warming (weakening) effect on the polar vortex. Meanwhile, accompanying the mature phase of the ENSO event, the warm and positive mass anomaly signal in the midlatitude stratosphere persists throughout the concurrent winter till the end of the next summer. These warming anomalies coupled with the delayed zonally homogeneous cooling anomalies in the midlatitude troposphere after the mature phase of a warm ENSO event, also exhibits a highly zonally homogeneous feature in the following spring-to-summer. In comparison with the concurrent winter, the wave-driven poleward heat transport by an anomalous wavenumber-2 is much stronger in the next winter season, resulting in the maximum warming and weakening of the stratospheric polar vortex accompanied with a colder midlatitude stratosphere.

In short, due to the delayed effect of a mature warm ENSO, warm temperature and positive isentropic mass anomalies persist in the midlatitude stratosphere from the preceding summer to the next summer. The warmer midlatitude stratosphere, plus the anomalous wave forcing in winter season, explains the warming and weakening effect of ENSO on the polar vortex in both of the concurrent winter and the next winter. However, the relatively weaker wave effect by the anomalous wavenumber-1 in the concurrent winter only results in a minor weakening of the stratospheric polar vortex. The much stronger wave effect by an anomalous wavenumber-2 in the next winter is responsible for the much warmer and weaker polar vortex accompanied with a colder midlatitude stratosphere.

Acknowledgments This work was supported by the National Basic Research Program of China (2010CB428603, 2010CB950400), the CAS under grant KZCX2-YW-Q11-01 and KZCX2-YW-BR-14. Ming Cai was supported by grants from the NOAA CPO/CPPA (NA10OAR4310168), National Science Foundation (ATM-0833001), and Department of Energy (DE-SC0004974). The authors also like to

thank the two anonymous reviewers for their constructive and insightful comments.

References

Angell JK (1981) Comparison of variations in atmospheric quantities with sea surface temperature variations in the Equatorial Eastern Pacific. Mon Wea Rev 109:230–243

Baldwin MP, Dunkerton TJ (2001) Stratospheric harbingers of anomalous weather regimes. Science 294:581–584

Cai M, Ren R-C (2006) 40–70 Day meridional propagation of global circulation anomalies. Geophys Res Lett. doi:10.1029/2005GL025024

Cai M, Ren R-C (2007) Meridional and downward propagation of atmospheric circulation anomalies. Part I: Northern Hemisphere cold season variability. J Atmos Sci 64:1880–1901

Calvo N, Giorgetta MA, Garcia-Herrera R, Manzini E (2009) Nonlinearity of the combined warm ENSO and QBO effects on the Northern Hemisphere polar vortex in MAECHAM5 simulations. J Geophys Res. doi:10.1029/2008JD011445

Camp CD, Tung KK (2007) Stratospheric polar warming by ENSO in winter: a statistical study. Geophys Res Lett. doi:10.1029/2006GL028521

Chen W, Takahashi M, Graf Hans-F (2003) Interannual variations of stationary planetary wave activity in the north winter troposphere and stratosphere and their relations to NAM and SST. J Geophys Res. doi:10.1029/2003JD003834

Davis RE (1976) Predictability of sea surface temperatures and sea level pressure anomalies over the North Pacific Ocean. J Phys Oceanogr 6:249–266

Ding RQ, Li JP (2011) Winter persistence barrier of sea surface temperature in the northern tropical Atlantic associated with ENSO. J Climate 24:2285–2299

Enfield DB, Mayer DA (1997) Tropical Atlantic sea surface temperature variability and its relation to El Niño-Southern Oscillation. J Geophys Res 102:929–945

García-Herrera R, Calvo N, Garcia RR, Giorgetta MA (2006) Propagation of ENSO temperature signals into the middle atmosphere: a comparison of two general circulation models and ERA-40 reanalysis data. J Geophys Res. doi:10.1029/2005JD006061

Garfinkel CI, Hartmann DL (2007) Effects of the El Niño–Southern Oscillation and the Quasi-Biennial Oscillation on polar temperatures in the stratosphere. J Geophys Res. doi:10.1029/2007JD008481

Garfinkel CI, Hartmann DL (2008) Different ENSO teleconnections and their effects on the stratospheric polar vortex. J Geophys Res. doi:10.1029/2008JD009920

Hamilton K (1993) An examination of observed southern oscillation effects in the northern hemisphere stratosphere. J Atmos Sci 50:3468–3474

Hamilton K (1995) Interannual variability in the northern hemisphere winter middle atmosphere in control and perturbed experiments with the GFDL SKYHI general circulation model. J Atmos Sci 52:44–66

Handoh IC, Matthews AJ, Bigg GR, Stevens DP (2006) Interannual variability of the tropical Atlantic independent of and associated with ENSO: Part I. The north tropical atlantic. Int J Climatol 26:1937–1956

Holton JR, Haynes PH, McIntyre ME, Douglass AR, Rood RB, Pfister L (1995) Stratosphere-troposphere exchange. Rev Geophys 33:403–439

Hsiung J, Newell RE (1983) The principal nonseasonal modes of variation of global sea surface temperature. J Phys Oceanogr 13:1957–1967

Hu Y, Tung KK (2002) Interannual and decadal variations of planetary wave activity, stratospheric cooling, and northern hemisphere Annular Mode. J Climate 15:1659–1673

Huang BH, Schopf PS, Pan ZQ (2002) The ENSO effect on the tropical Atlantic variability: a regionally coupled model study. Geophys Res Lett 29. doi:10.1029/2002GL014872

Itoh H, Harada K (2004) Coupling between tropospheric and stratospheric leading modes. J Climate 17:320–336

Johnson DR (1989) The forcing and maintenance of global monsoonal circulations: an isentropic analysis. Adv Geophys 31:43–316

Katz RW (1982) Statistical evaluation of climate experiments with general circulation models: a parametric time series modeling approach. J Atmos Sci 39:1446–1455

Klein SA, Soden BJ, Lau NC (1999) Remote sea surface temperature variations during ENSO: evidence for a tropical atmospheric bridge. J Climate 12:917–932

Kumar A, Hoerling MP (2003) The nature and causes for the delayed atmospheric response to El Niño. J Climate 16:1391–1403

Labitzke K, Hvan Loon (1989) The Southern Oscillation. Part IX: the influence of volcanic eruptions on the Southern Oscillation in the stratosphere. J Climate 2:1223–1226

Lanzante JR (1996) Lag relationships involving tropical sea surface temperatures. J Climate 9:2568–2578

Lau NC, Nath MJ (2003) Atmosphere–ocean variations in the Indo-Pacific sector during ENSO episodes. J Climate 16:3–20

Lau NC, Leetmaa A, Nath MJ, Wang HL (2005) Influences of ENSO-induced Indo–Western Pacific SST anomalies on extratropical atmospheric variability during the boreal summer. J Climate 18:2922–2942

Manzini E, Giorgetta MA, Esch M, Kornblueh L, Roeckner E (2006) The influence of sea surface temperatures on the northern winter stratosphere: ensemble simulations with the MAECHAM5 model. J Climate 19:3863–3881

Mohanakumar K (2008) Stratosphere troposphere interaction: an introduction. Springer Science + Business Media B. V.

Newell RE, Weare BC (1976) Factors governing tropospheric mean temperature. Science 194:1413–1414

Pan YH, Oort AH (1983) Global climate variations connected with sea surface temperature anomalies in the Eastern Equatorial Pacific ocean for the 1958–1973 period. Mon Wea Rev 111:1244–1258

Plumb RA, Eluszkiewicz J (1999) The Brewer–Dobson circulation: dynamics of the tropical upwelling. J Atmos Sci 56:868–890

Reid G, Gage K, McAfee J (1989) The thermal response of the tropical atmosphere to variations in Equatorial Pacific sea surface temperature. J Geophys Res 94:14705–14706

Ren R-C, Cai M (2007) Meridional and vertical out-of-phase relationships of temperature anomalies associated with the Northern Annular Mode variability. Geophys Res Lett. doi:10.1029/2006GL028729

Ren R-C, Cai M (2008) Meridional and downward propagation of atmospheric circulation anomalies. Part II: Southern Hemisphere cold season variability. J Atmos Sci 65:2343–2359

Reynolds RW, Rayner NA, Smith TM, Stokes DC, Wang W (2002) An Improved in situ and satellite SST analysis for climate. J Climate 15:1609–1625

Saravanan R, Chang P (2000) Interaction between tropical Atlantic variability and El Niño-Southern Oscillation. J Climate 13:2177–2194

Sassi F, Kinnison D, Boville BA, Garcia RR, Roble R (2004) Effect of El Niño–Southern Oscillation on the dynamical, thermal, and chemical structure of the middle atmosphere. J Geophys Res. doi:10.1029/2003JD004434

Taguchi M, Hartmann DL (2006) Increased occurrence of stratospheric sudden warmings during el niño as simulated by WACCM. J Climate 19:324–332

Thompson DW, Wallace JM (2000) Annular modes in the extratropical circulation. Part I: Month-to-Month Variability. J Climate 13:1000–1016

Trenberth KE (1984) Some effects of finite sample size and persistence on meteorological statistics. Part I: autocorrelations. Mon Wea Rev 112:2359–2368

Uppala SM, KÅllberg PW, Simmons AJ et al (2005) The ERA-40 reanalysis. Quart J R Meteorol Soc 131:2961–3012

van Loon H, Labitzke K (1987) The Southern Oscillation. Part V: the anomalies in the lower stratosphere of the northern hemisphere in winter and a comparison with the Quasi-Biennial Oscillation. Mon Wea Rev 115:357–369

van Loon H, Zerefos C, Repapis C (1982) The Southern Oscillation in the stratosphere. Mon Wea Rev 110:225–229

Wallace JM, Chang FC (1982) Interannual variability of the wintertime polar vortex in the Northern Hemisphere middle stratosphere. J Meteor Soc Jpn 60:149–155

Wei K, Chen W, Huang R (2007) Association of tropical Pacific sea surface temperatures with the stratospheric Holton-Tan Oscillation in the Northern Hemisphere winter. Geophys Res Lett. doi: 10.1029/2007GL030478

Yulaeva E, Wallace JM (1994) The signature of ENSO in global temperature and precipitation fields derived from the microwave sounding unit. J Climate 7:1719–1736